Proceedings of the ASME 2021
International Mechanical Engineering Congress and Exposition
IMECE2021
November 1-4, 2021, Virtual, Online

IMECE2021-69467

FLOW DISTURBANCE GENERATORS BASED ON OSCILLATING CYLINDERS WITH ATTACHED SPLITTER PLATES

Michael Hughes
North Carolina State University
Raleigh, NC

Mariah Mook
North Carolina State University
Raleigh, NC

Michael Jenkins
North Carolina State University
Raleigh, NC

Arun Vishnu SureshBabu
North Carolina State University
Raleigh, NC

Ashok Gopalarathnam
North Carolina State University
Raleigh, NC

Matthew Bryant
North Carolina State University
Raleigh, NC

ABSTRACT

The interaction between upstream flow disturbance generators and downstream aeroelastic structures has been the focus of several recent studies at North Carolina State University. Building on this work, which observed the modulation of limit cycle oscillations (LCOs) in the presence of vortex wakes, this study examines the design and validation of a novel disturbance generator consisting of an oscillating cylinder with an attached splitter plate. Analytical design of the bluff body was performed based on specific flow conditions which produced LCO annihilation in previous studies. Computational fluid dynamics simulations and experimental wind tunnel tests were used to validate the ability of the new disturbance generator to produce the desired wake region. Future work will see the implementation of this novel design in conjunction with aeroelastic structures in an effort to modulate and control LCOs, including the excitation and annihilation thereof.

Keywords: limit cycle oscillations, aeroelasticity, bluff body disturbance generator, CFD, wind tunnel, fluid-structure interaction

NOMENCLATURE

A	Bluff body pitch amplitude
B	Constant for King's Law
C	Constant for King's Law
D	Diameter
f_{shed_n}	Cylinder natural shedding frequency
f_{osc}	Bluff body oscillation frequency
n	Constant for King's Law
St	Strouhal number
St_n	Natural Strouhal number
u_∞	Freestream velocity
u	Velocity

1. INTRODUCTION

Fluid-elastic structures exhibit two-way coupling between the fluidic and structural domains; hence, the motion dynamics are dictated by both the structural and the flow parameters. Prior efforts at modifying the fluid-structure interaction behaviors of aeroelastic wings have predominantly focused on changing structural parameters or changing the structure's aerodynamic characteristics, rather than introducing and exploiting disturbances in the flow field itself. For example, prior research on controlling aeroelastic limit cycles and flutter behavior have used movable control surface flaps [1] [2] or morphing that is aimed at increasing vehicle performance by manipulating structural [3] [4] and aerodynamic characteristics of the wing to better match the vehicle state to the environment and task at hand. The former method has been more commonly investigated

because flap control surfaces are well established mechanisms for other aspects of flight control [1].

Recent work by the Aeroelasticity Group at North Carolina State University (NCSU) has demonstrated that aeroelastic stability and limit cycle oscillation (LCO) behavior can be modified by upstream flow disturbances. Aircraft wings, which are practical examples of common aeroelastic systems, have been shown to experience LCOs in both undisturbed and perturbed flows, the latter having been the focus of recent work by the Aeroelasticity Group at NCSU. Initially, the interaction between a pair of in-line, aeroelastic wings was examined by Kirschmeier and Bryant [5]. It was found that the wake produced by the upstream wing experiencing LCOs led to destabilization of the downstream wing, resulting in sustained oscillations at wind speeds below the freestream flutter speed of the downstream wing. Following this work, Gianikos et al. [6] replaced the upstream wing with a static, rectangular, bluff body which produced periodic vortices in its wake. As vortices shed by the bluff body impinged on the aeroelastic wing section, already experiencing LCOs, the LCO amplitude was periodically modulated due to the interaction between the aeroelastic wing section and the vortices. Most recently, Kirschmeier et al. [7] found that the LCOs could be completely annihilated in the downstream wing when the shedding frequency of the bluff body was equal to three times the oscillation frequency of the LCOs.

Following the completion of these studies and the discovery of the LCO annihilation, the ability to control the frequency and phase of vortices shed by the upstream disturbance generator at constant flow speed was desired. In the process of designing a new upstream disturbance generator, it was decided to pursue cylindrical bluff bodies due to their well-studied ability to produce von Kármán vortices [8]. However, a simple, static cylinder does not allow for variation of the vortex shedding frequency and phase as its vortex shedding frequency is dependent on the freestream velocity and cylinder diameter, as described by the Strouhal number property. Rockwood and Medina [9], found that by inducing prescribed pitch oscillations about the primary axis of the cylinder, the vortex shedding frequency can be altered. Additionally, by adding an attached splitter plate along the trailing edge of the cylinder, Rockwood and Medina [9] found that the shedding frequency can be prescribed at the cylinder's oscillation frequency and produce a well-behaved, locked-in, von Kármán vortex street.

Building on the experimental work done by Rockwood and Medina, Chatterjee et al. [10] performed a CFD analysis to examine the behavior of the vortex wake across a range of Strouhal ratios, that is, the ratio of the Strouhal number due to the forced vortex shedding frequency when compared to the Strouhal number due to the natural shedding frequency of a cylinder of the same diameter without an attached splitter plate. Their results suggested that a cylindrical bluff body with an attached splitter plate produced a well-behaved, locked-in, vortex wake when the Strouhal ratio fell between 0.8 and 1.4. At values above 1.4, the time between each shed vortex was inconsistent, resulting in undesirable variation in control of the system wake when considered for application in conjunction with downstream aeroelastic structures.

Based on the information presented in the brief review above, it was decided to move forward with the cylindrical bluff body design with an attached splitter plate in order to continue investigation of aeroelastic LCO modulation and control. A design requirement for the system was to demonstrate maximum cylinder oscillation frequencies of at least three times the LCO frequency of the existing aeroelastic wing section apparatus under conditions where LCO annihilation has been demonstrated [7].

The work done by Rockwood and Medina [9] and Chatterjee et al. [10] was performed with in a water tunnel apparatus at Reynolds numbers of 7600 based on the cylinder diameter. This differs from the earlier work done by the Aeroelasticity Group at NCSU which was performed in the NCSU subsonic wind tunnel at airfoil-chord-based Reynolds numbers ranging from 70000 to 120000. As a result, the work presented in this paper was completed with the goal of experimentally validating the Strouhal ratio range described by Chatterjee et al. [10] for applications in future aeroelasticity work in the NCSU subsonic wind tunnel.

2. MATERIALS AND METHODS

2.1 Bluff Body Sizing

The design process used to generate the bluff body for the work outlined in this paper is focused on a set of design parameters based on previous research done in the Aeroelasticity Group at NCSU. The primary design goal is to produce a bluff body which sheds vortices at a rate which corresponds to the range of Strouhal ratios as discussed in Chatterjee et al [10]. For a standard, static cylinder, the natural Strouhal number can be found by:

$$St_n = \frac{f_{shed_n} D}{u_\infty} \tag{1}$$

For cylinders which fall in the Reynolds number range $1000 \leq Re \leq 100{,}000$, this value is approximately $St_n = 0.2$ [8]. To calculate the Strouhal ratio, St/St_n, the Strouhal number for the oscillating cylinder and splitter plate is calculated by setting the frequency of the shed vortices to the oscillation frequency of the body, while the freestream velocity and the cylinder diameter as equivalent to the values used in the natural Strouhal number calculations.

$$St = \frac{f_{osc} D}{u_\infty} \tag{2}$$

From these two equations, the oscillation frequency of the bluff body can be calculated by:

$$f_{osc} = St_n \left(\frac{St}{St_n}\right) \frac{u_\infty}{D} \tag{3}$$

treating the Strouhal ratio as a single variable. Sweeping through the range of acceptable Strouhal ratios discussed in Chatterjee et al. [10], a range of oscillation frequencies can be found for any given flow conditions and cylinder diameter. Conversely, the oscillation frequency can be prescribed and a range of acceptable cylinder diameters can be calculated. In order to achieve oscillation frequencies equal to three times the LCO frequency for cases similar to previous work done in the Aeroelasticity Group at NCSU, the parameters shown in Table 1 were generated.

TABLE 1. Cylinder Sizing

St/St_n	$f_{osc}\ (Hz)$	$u_\infty (m/s)$	$D\ (cm)$
0.8	12	8	10.67
0.9	12	8	12.00
1.0	12	8	13.33
1.1	12	8	14.67
1.2	12	8	16.00
1.3	12	8	17.33
1.4	12	8	18.67

From this list of possible cylinder diameters, an initial value of $D = 10.67\ cm$ was chosen as the design point. However, due to construction constraints and available materials, a final diameter of $D = 10.48\ cm = 4.125\ in.$ was selected. A cross section of the bluff body geometry is shown in Figure 1.

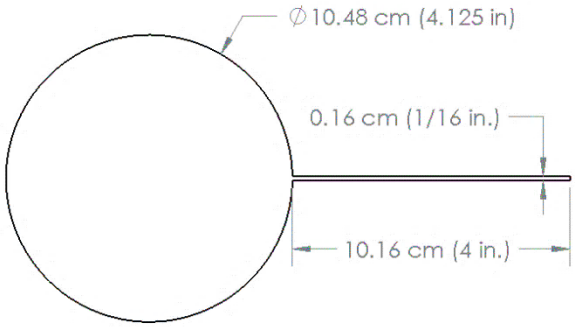

FIGURE 1. Bluff body design geometry.

2.2 CFD Simulations

Following the initial design for the new bluff body, a series of CFD simulations were run to validate the ability of the chosen bluff body configuration to generate a well-behaved von Kármán vortex street at the flow conditions of interest. An O-type structured grid was fitted to the bluff body. The velocity-inlet and pressure-outlet boundaries were both located at a distance of 25 cylinder diameters away from the rotational center of the bluff body. The domain was partitioned into an inner and outer region so that sinusoidal rotation of the bluff body did not result in mesh deformation. The bluff body contained 660 elements along its surface, resulting in the inner region containing 148500 elements. A total of 163500 elements were used in the entire domain. A first layer cell height of 1.5e-5 m ensured a y^+ value below 1 over the entirety of the bluff body surface.

Simulations were performed using the commercial package Fluent 20.1. The SST k-ω turbulence model was chosen due to the problem involving large extents of separated flow, with the downstream wake being the primary interest. The proposed Reynolds numbers and chosen oscillatory speeds do not allow a laminar flow regime to be assumed, as doing so leads to a highly disorganized and chaotic wake not associated with the results of previous experiments. The decision to use the SST k-ω model is further supported by the work performed by Chatterjee et al. [10], in which the SST k-ω model was used with an intermittency transition model to successfully replicate the vortex street produced by water tunnel experiments. Later efforts contrasting the inclusion and exclusion of the transition model revealed that its absence did not significantly affect the wake produced by the oscillating bluff body. The removal of the transition model also led to a notable reduction in computational time. For these reasons stated, the authors have decided to implement the SST k-ω model in the present CFD simulations. The SIMPLE algorithm was chosen for the pressure-velocity coupling scheme, and a static timestep of 5e-5 seconds was used for all five cases. Absolute residuals were driven to below 7e-5 at each timestep.

2.3 Bluff Body Construction

The main body of the cylinder was constructed of braided, carbon fiber tubing produced by DragonPlate™ (Elbridge, NY, USA) with a 45° fiber orientation. A vertical cut was made from one end of the tube to allow the splitter plate sub-assembly to be inserted during construction.

The splitter plate, shown in Figure 2, was constructed of aluminum in previous design iterations, but added a significant amount of mass and inertia due to its location away from the axis of rotation. To reduce its mass and inertia while maintaining stiffness, a 1/16” thick, carbon fiber and birch laminate produced by DragonPlate™ was selected as a replacement. The laminate is constructed of a solid birch core laminated between two thin sheets of carbon fiber. This allows for a stiff, yet lightweight material, thereby reducing the inertial effects from the splitter plate in the final bluff body configuration. Additionally, the splitter plate was inset into the cylinder and supported using a series of aluminum baffles to further improve stiffness and ensure minimum deformation when the bluff body is oscillating. A series of aluminum baffles of similar design to the splitter plate supports were constructed to support the carbon fiber cylinder and attach mounting shafts. When operated in the wind tunnel, the bluff body is supported at the top with a flexible shaft collar which helps correct for small misalignment errors. The bluff body is then connected to a motor shaft using a rigid shaft collar at the bottom. An exploded view diagram of the bluff body construction can be seen in Figure 3.

2.4 Testing Apparatus

In conjunction with the computational simulations, a series of experiments were performed in the NCSU closed-return, subsonic wind tunnel, which has a test section measuring 0.81 m × 1.14 m × 1.17 m. Experimental tests were set to match the freestream velocities, bluff body oscillation profiles, and downstream velocity measurement locations as those in the CFD simulations.

The motor selected to drive the oscillation of the bluff body was a SureServo SVL-210b from AutomationDirect (Cumming, GA, USA) with a maximum continuous torque of 3.3 Nm and a maximum instantaneous torque of 9.9 Nm. This was coupled with a Copley Controls (Canton, MA, USA) Xenus XTL-230-18 digital servo drive to provide motor control via Copley Controls CME 2.0. In addition to direct control through the CME 2.0 software, the motor was driven using the Xenus' onboard function generator and queried over serial communication within a LabVIEW VI running on a National Instruments (Austin, TX, USA) PXI data acquisition system. In both cases, the Xenus supplies a sinusoidal trajectory with user defined frequency and amplitude to drive the oscillation of the disturbance generator which is displayed in Figure 4.

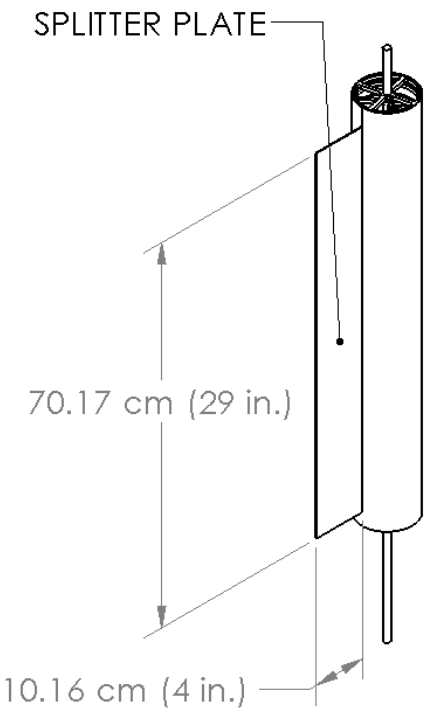

FIGURE 2. Splitter plate diagram with dimensions.

Velocity data during testing was acquired using a MiniCTA 54T30 and a straight, miniature wire probe (55P11) manufactured by Dantec Dynamics (Skovlunde, Denmark). Measurements were recorded at a distance of six diameters downstream of the oscillating bluff body, as shown in Figure 5, to obtain averaged velocities in the wake. For hot-wire calibration, ten sample points were recorded at dynamic pressures of 4.79 Pa to 47.9 Pa (0.1 to 1.0 psf) at the test section centerline before the disturbance generator was placed in the wind tunnel. Following King's Law:

$$E^2 = B + Cu^n \tag{4}$$

the average voltage at each dynamic pressure were fitted to a curve to determine the calibration coefficients B and C, while $n = 0.45$. These coefficients were used to convert the voltage data obtained by the hotwire into velocities. During the experiment, the bluff body was installed upstream and the hotwire probe support was traversed at increments of 1.27 cm (0.5 in.) up to 20.32 cm (8.0 in.) on either side of the centerline to characterize the full wake generated by the bluff body.

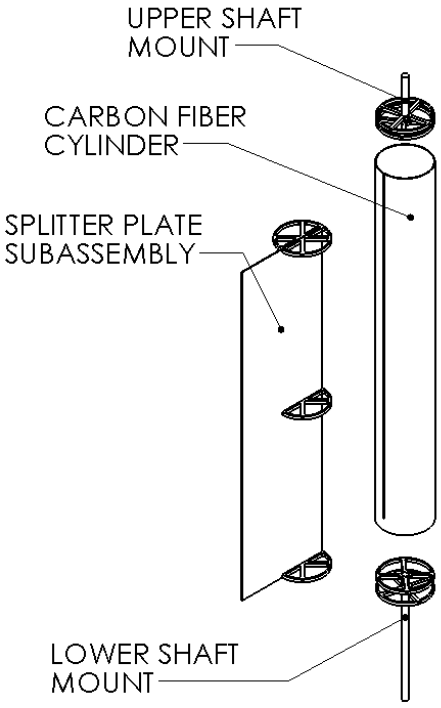

FIGURE 3. Bluff body exploded view.

2.5 Test Cases

While the design for the cylindrical bluff body, discussed in Section 2.3, was optimized for oscillation at 12 Hz with a freestream velocity of 8 m/s and $St/St_n = 0.8$, alternative testing conditions, shown in Table 2, allowed for a full sweep of Strouhal ratios ranging from 0.8 to 1.4. Additionally, one case outside the acceptable range of Strouhal ratios determined for Re = 7600 was included to observe whether different wake behavior would occur at the higher Reynolds number case considered here.

TABLE 2. Wind Tunnel Test Cases

St/St_n	$f_{osc}\ (Hz)$	$A\ (°)$	$u_\infty (m/s)$	$D\ (cm)$
0.66	4	15	3.25	10.48
0.82	5	15	3.25	10.48
0.98	6	15	3.25	10.48
1.15	7	15	3.25	10.48
1.31	8	15	3.25	10.48

Data gathered during testing included rotational position of the oscillating bluff body and downstream velocity as functions of time. Rotational position data was gathered using the encoder on the SVL-210b motor, transmitted via RS-232 cable, and recorded using LabVIEW. Velocity data was gathered with the hot-wire probe, transmitted via BNC cable, and recorded using LabVIEW.

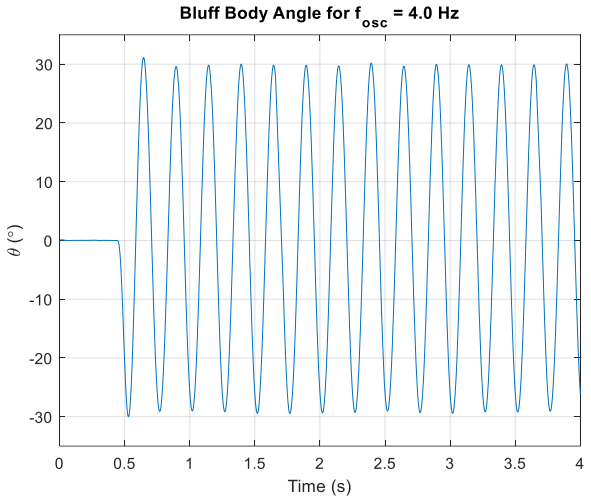

FIGURE 4. Bluff body rotation for an input frequency and amplitude of 4 Hz and 30° respectively.

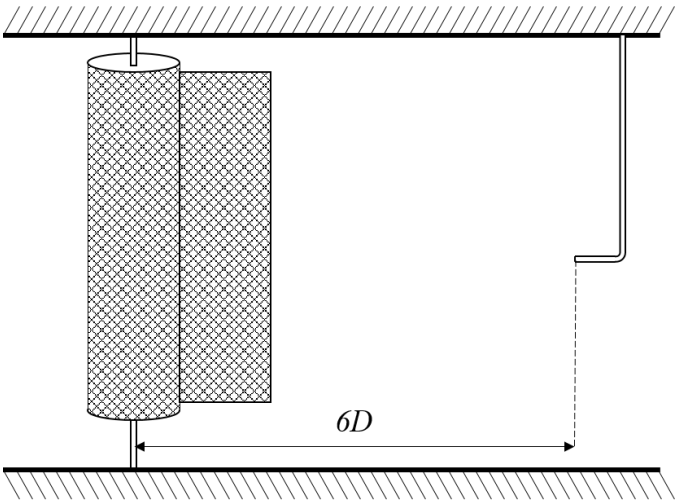

FIGURE 5. Location of downstream hotwire probe.

3. RESULTS AND DISCUSSION

Upon completion of both CFD and experimental testing, the results were post-processed using MATLAB 2020a.

3.1 CFD Results

In the CFD simulations, velocity in the streamwise direction at a location $6D$ downstream from the bluff body was recorded for the duration of the simulation. In order to remove the transient effects produced when the bluff body initially begins to rotate, the first two seconds of velocity data were excluded for all calculation. The remaining data, shown in Figure 6, produced a well-defined, cyclical velocity profile which correlates to the passing of regularly space vortex structures.

Additionally, flow visualization data, shown in Figure 7, displays well-defined, vortex wakes for each of the test cases discussed in Table 2. The 4 Hz case, which fell outside the range of acceptable Strouhal ratios at Re = 7600, also appears to produce well-organized wake at the higher Reynolds number case simulated here.

Fast Fourier Transforms (FFT) were used to quantify the vortex shedding frequency of the bluff body from the simulation results. The downstream velocity data, shown in Figure 6, was analyzed with an FFT in MATLAB. Since one oscillation of the bluff body constitutes both an upward and downward motion of the bluff body, two vortices are produced with opposite spin direction, which can be seen in the vorticity contours in Figure 7. As a result, the FFT, shown in Figure 8, displays frequency peaks at a rate of twice the oscillation frequency.

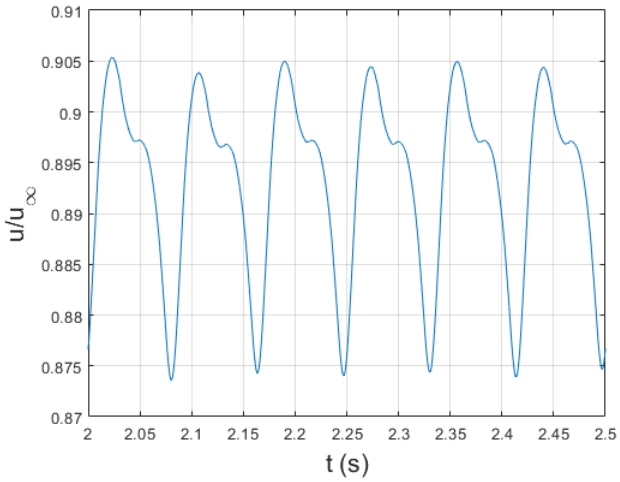

FIGURE 6. Downstream velocity trace for f_{osc} = 6 Hz.

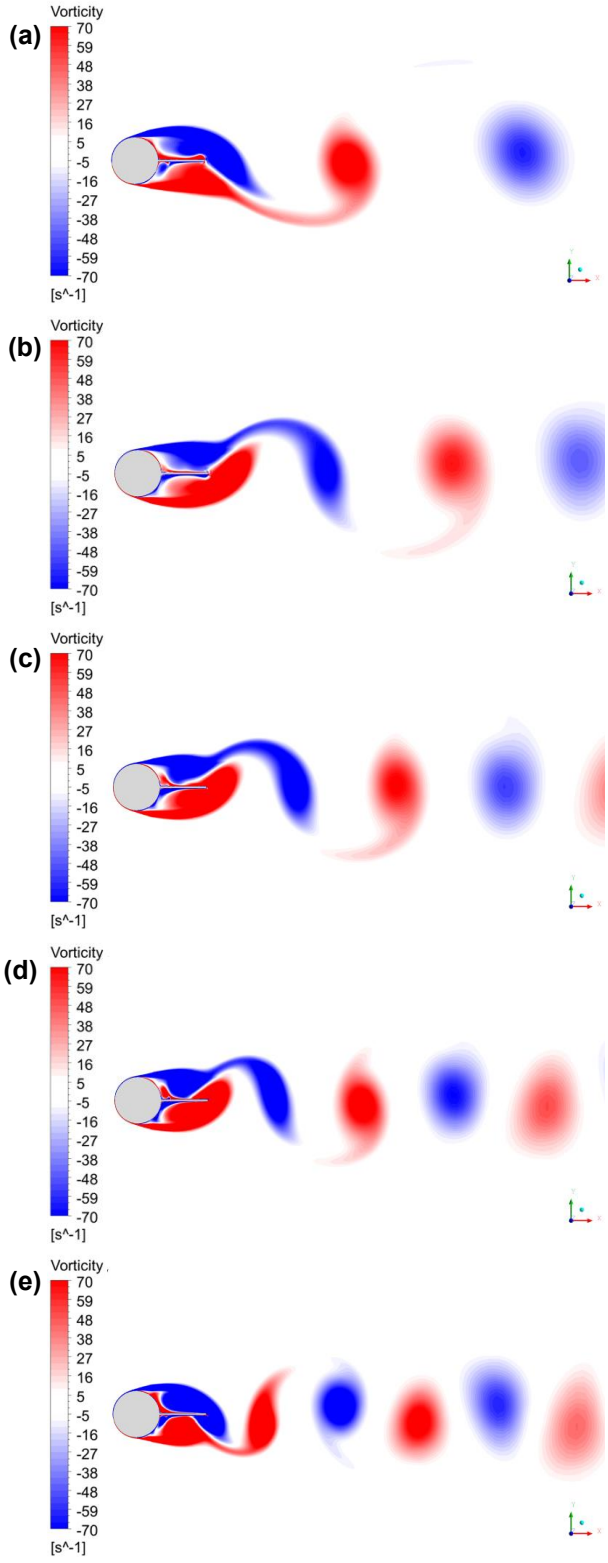

FIGURE 7. Vorticity contours from CFD showing well-defined vortex wakes for oscillation frequencies of (a) 4 Hz, (b) 5 Hz, (c) 6 Hz, (d) 7 Hz and (e) 8 Hz.

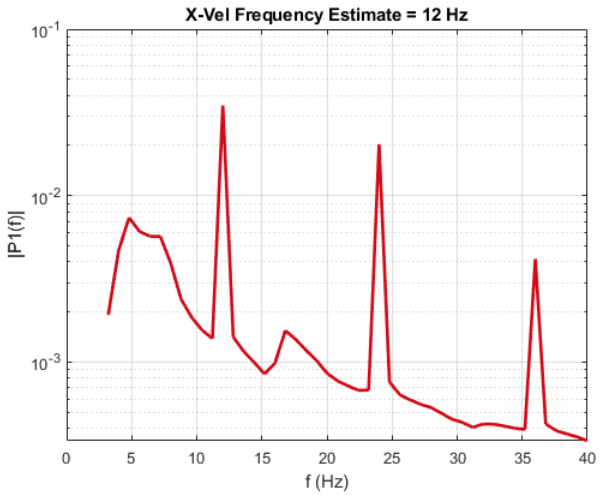

FIGURE 8. Frequency spectrogram for oscillation frequency of 6 Hz, showing an initial peak at 12 Hz as expected.

3.2 Experimental Results

Data gathered via hot wire anemometry during the experimental tests was time-averaged for each of the oscillation frequency cases shown in Table 2 and plotted as a function of cross-stream distance from the test section centerline at increments of y/D = 1/8. All test cases display a clear wake velocity deficit region, as shown in Figure 9, but the shape and magnitude of the velocity variation across the flow varied strongly with the oscillation frequency of the bluff body. The results indicate that, for the cases tested here, higher oscillation frequencies produce a larger centerline velocity deficit, and also show a sharper variation in velocity across the flow.

Data analysis comparing opposite cross-stream locations away from the test section centerline show some asymmetry in the time-averaged velocity profile. At y/D = 1, as shown in Figure 10, for higher oscillation frequencies the difference in time-averaged velocity between points equidistant from the centerline is magnified. The reason for this is currently unknown and could be the result of a cross-stream shift in the wake region produced by the bluff body. However, at y/D = 2, the values are much more similar, due in large part to these values approaching the freestream velocity.

3.3 CFD and Experimental Comparison

While data gathered during experimental testing provided velocity profiles extending away from the test section centerline, computational velocities were only computed at the centerline. In order to compare the two methods, the time-averaged velocity at the centerline from each method was plotted as a function of oscillation frequency, as shown in Figure 11.

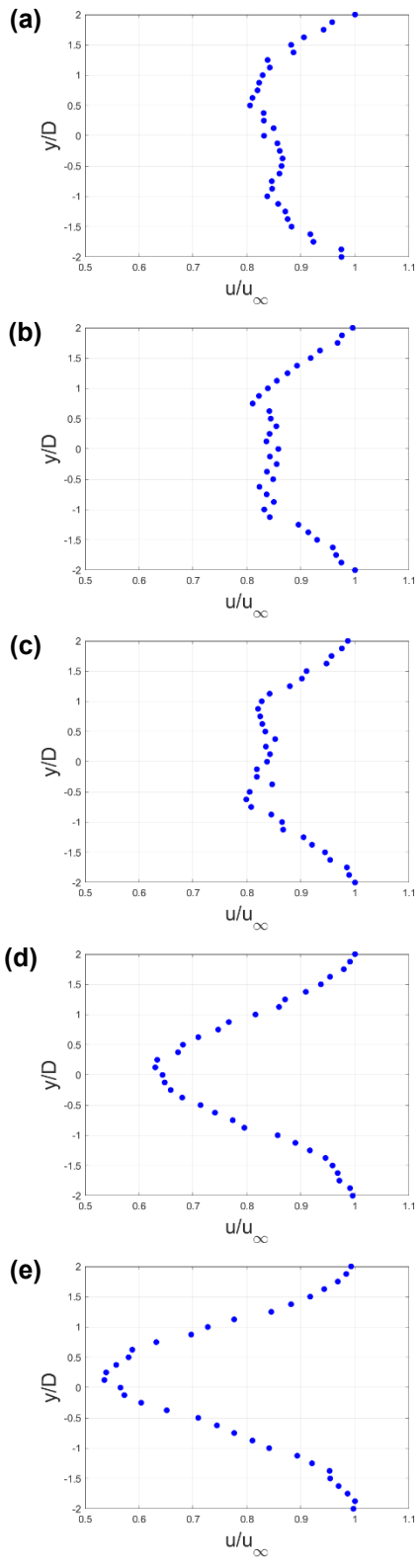

FIGURE 9. Cross-stream, time-averaged velocity profiles for (a) 4 Hz, (b) 5 Hz, (c) 6 Hz, (d) 7 Hz and (e) 8 Hz.

While the time-averaged velocities show agreement for the lower oscillation frequencies, the experimental data shows a sharp decrease beginning at $f_{osc} = 7\ Hz$. Explanations for this significant variation from the simulated cases could be due to inconsistencies in the experimental testing apparatus that are only present at these higher oscillation frequencies. Additionally, the SST k-ω turbulence model used for the CFD simulations may have failed to capture all of the turbulent effects produced in the physical tests.

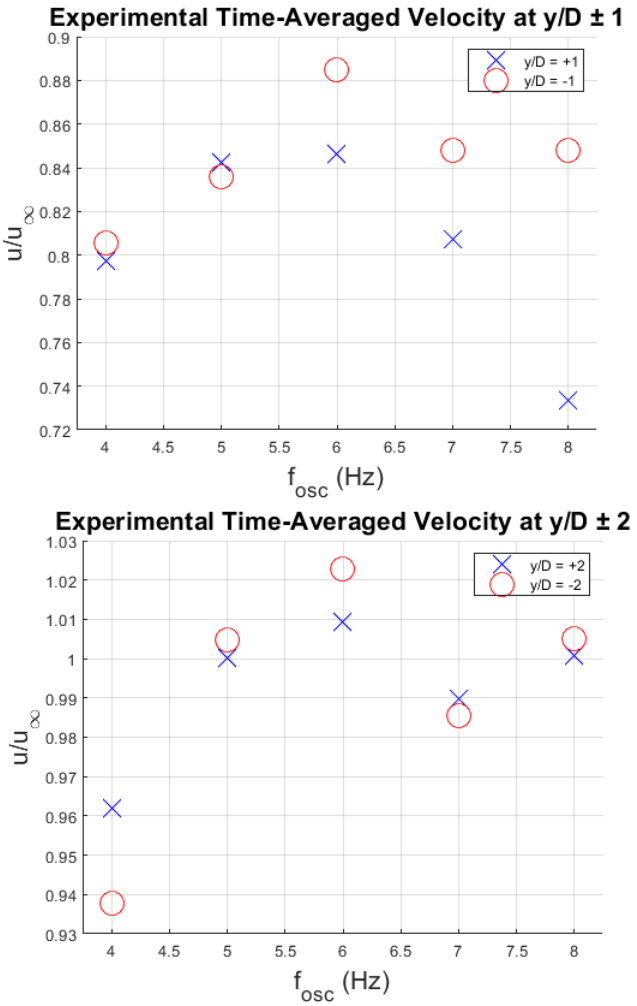

FIGURE 10. Average velocities with increasing oscillation frequencies showing asymmetries in the vortex wake.

4. CONCLUSION

In this paper, a cylindrical bluff body with an attached splitter plate was designed to serve as a disturbance generator to produce a well-defined, von Kármán vortex street with variable frequency at a constant flow speed. Based on preliminary results from both computational and experimental methods, this configuration succeeds in producing the desired wake at frequencies corresponding to 0.8 to 1.4 times the frequency of

natural vortex shedding for a plain cylinder at the same speed. Future studies will seek to examine the frequency content produced by the disturbance generator at a wide range of x/D and y/D locations to further characterize the wake region using a wide array of computational and experimental techniques.

TABLE 3. Percent difference in velocity at equidistant cross-stream locations.

f_{osc}	$y/D = \pm 1$	$y/D = \pm 2$
4	1.03%	2.51%
5	0.80%	0.44%
6	4.56%	1.35%
7	5.04%	0.43%
8	15.63%	0.43%

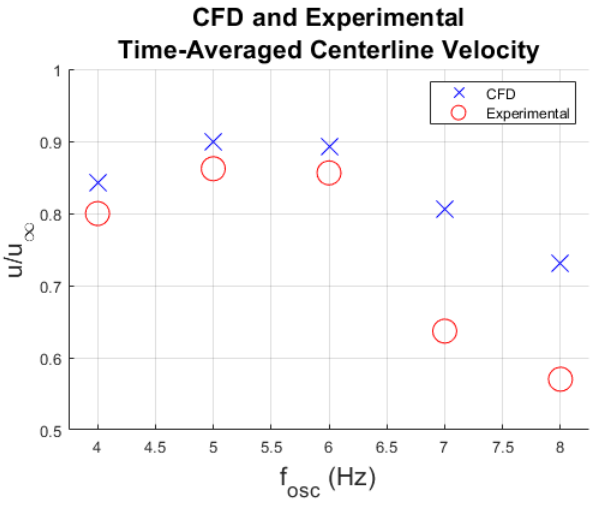

FIGURE 11. Comparison between computational and experimental centerline average velocities.

ACKNOWLEDGEMENTS

The authors gratefully acknowledge funding support for this research from the National Science Foundation under Award No. CMMI-2015983 and program officer Dr. Robert Landers. Additionally, this work also includes, and is based upon research supported by the Air Force Office of Scientific Research under award number FA9550-17-1-0301, monitored by Dr. Gregg Abate.

REFERENCES

[1] Strganac, T. W., Ko, J., Thompson, D., and Kurdila, A., 2000, "Identification and control of limit cycle oscillations in aeroelastic systems," J. Guid. Control Dyn., **23**(6), pp. 1127–1133.

[2] Shukla, H., and Patil, M. J., 2017, "Controlling Limit Cycle Oscillation Amplitudes in Nonlinear Aeroelastic Systems," J. Aircr., **54**(5), pp. 1921–1932.

[3] Tsushima, N., and Su, W., 2017, "Flutter suppression for highly flexible wings using passive and active piezoelectric effects," Aerosp. Sci. Technol., **65**, pp. 78–89.

[4] Timpe, A., Zhang, Z., Hubner, J., Ukeiley, L., 2013, "Passive flow control by membrane wings for aerodynamic benefit Topics in Flow Control. Guest editors J.P. Bonnet and L. Cattafesta," Exp. Fluids, **54**(3).

[5] Kirschmeier, B., and Bryant, M., 2018, "Experimental Investigation of Wake-Induced Aeroelastic Limit Cycle Oscillations in Tandem Wings," Journal of Fluids and Structures, **81**, pp. 309-324.

[6] Gianikos, Z. N., Kirschmeier, B. A., Gopalarathnam, A., and Bryant, M., 2020, "Limit Cycle Characterization of an Aeroelastic Wing in Bluff Body Wake," Journal of Fluids and Structures, **95**, 102986.

[7] Kirschmeier, B. A., Gianikos, Z., Gopalarathnam, A., and Bryant, M., 2020, "Amplitude Annihilation in Wake-Influenced Aeroelastic Limit-Cycle Oscillations," AIAA Journal, **58**(9).

[8] Williamson, C. H. K., 1996, "Vortex Dynamics in the Cylinder Wake," Annual Review of Fluid Mechanics, **28**(1), pp. 477-539.

[9] Rockwood, M., and Medina, A., 2020, "Controlled Generation of Periodic Vortical Gusts by the Rotational Oscillation of a Circular Cylinder and Attached Plate," **61**(65).

[10] Chatterjee, P., Jenkins, M., SureshBabu, A. V., Medina, A., Gopalarathnam, A., Bryant, M., "Tailored Bluff Body Motion for Generating Desired Wake Structures," *AIAA AVIATION 2020 FORUM*, 2020.